Electric Field Controlled Self-Assembly of Hierarchically Ordered Membranes

*Yuri S. Velichko, Jason R. Mantei, Ronit Bitton, Daniel Carvajal, Kenneth R. Shull, and Samuel I. Stupp**

Self-assembly in the presence of external forces is an adaptive, directed organization of molecular components under nonequilibrium conditions. While forces may be generated as a result of spontaneous interactions among components of a system, intervention with external forces can significantly alter the final outcome of self-assembly. Superimposing these intrinsic and extrinsic forces provides greater degrees of freedom to control the structure and function of self-assembling materials. In this work we investigate the role of electric fields during the dynamic self-assembly of a negatively charged polyelectrolyte and a positively charged peptide amphiphile in water leading to the formation of an ordered membrane. In the absence of electric fields, contact between the two solutions of oppositely charged molecules triggers the growth of closed membranes with vertically oriented fibrils that encapsulate the polyelectrolyte solution. This process of self-assembly is intrinsically driven by excess osmotic pressure of counterions and the electric field is found to modify the kinetics of membrane formation as well as membrane morphology and properties. Depending on the strength and orientation of the field we observe a significant increase or decrease of up to nearly 100% in membrane thickness, or the controlled rotation of nanofiber growth direction by 90 degrees which leads to a significant increase in mechanical stiffness. These results suggest the possibility of using electric fields to control structure in self-assembly processes that involve the diffusion of oppositely charged molecules.

1. Introduction

Spontaneous self-assembly into a state of thermodynamic equilibrium should lead to materials with properties that are independent of kinetic pathway.[1a–e] Many strategies have been developed to control this process including molecular design,[1b] dilution,[2] kinetics,[3] the addition of thermal energy,[4] and change of the pH,[5] to name a few. In contrast to spontaneously self-assembling artificial systems, many biological structures dissipate energy in order to maintain the organized state. For example, tubulin[6] and actin[7] are known to form cytoskeletal filaments that give structural integrity to the cell and perform important functions. This dissipative self-assembly is a nonequilibrium thermodynamic process that requires a constant supply of energy to maintain both the process and resulting products in a steady state. Dissipative systems can exhibit characteristic collective effects[8] and may form complex symmetrical structures[9] or exhibit spatiotemporal patterns.[10] The use of external energy sources in dissipative systems suggests new ways to intervene to build structures. In this work we have investigated the role of electric fields in a dissipative process of self-assembly between oppositely charged macromolecules and small molecules. The system studied here was recently discovered in our laboratory[11] and involves the dynamic self-assembly of a hierarchically ordered membrane at the interface between dilute aqueous solutions of high molecular weight negatively charged hyaluronic acid (HA) and positively charged self-assembling peptide amphiphiles (PAs).[11] These PAs consist of an alkyl tail, an amino acid sequence with propensity for β-sheet formation and a positively charged terminal sequence.[12a–c] The high propensity of the molecules to form β-sheets along with hydrophobic collapse of alkyl tails yields the formation of high-aspect ratio cylindrical nanofibers.[13a,b] When the two liquids are brought into contact, electrostatic complexation between PA and HA molecules results in the rapid formation of a dense fibrous layer at the liquid-liquid interface that acts as a diffusion barrier and prevents further mixing of molecules. However, the chemical equilibrium in each compartment is disturbed not

Dr. Y. S. Velichko,[+] J. R. Mantei,[+] Dr. D. Carvajal, K. R. Shull, Prof. S. I. Stupp
Department of Materials Science and Engineering
Northwestern University
2220 Campus Drive, Evanston, Illinois 60208
E-mail: s-stupp@northwestern.edu
Prof. S. I. Stupp
Department of Chemistry
Northwestern University
2220 Campus Drive, Evanston, Illinois 60208
Prof. S. I. Stupp
Department of Medicine
Northwestern University
2220 Campus Drive, Evanston, Illinois 60208
Dr. R. Bitton, Prof. S. I. Stupp
Institute for BioNanotechnology in Medicine
Northwestern University
Chicago, Illinois 60611
[+] Y.S.V. and J.R.M contributed equally to this work

DOI: 10.1002/adfm.201101538

only at the interface, but in the entire volume. The solution of high molecular weight polyelectrolytes has a natural propensity for small ion accumulation.[14] This leads to an imbalance of ionic osmotic pressure between the PA and HA compartments separated by the diffusion barrier in analogy to the Donnan effect.[15] The appearance of this new force drastically changes the course of molecular diffusion and aggregation. Excess osmotic pressure stops the diffusion of small PA molecules and aggregates and promotes instead the reptation of long HA chains through the diffusion barrier and into the PA compartment. This process nucleates the formation of complexed PA-HA nanofibers (**Figure 1**A) perpendicular to the interface which grow longer with time.[11]

Given the importance of charged components in our system and the dynamic origin of the process driven by an aggregation-diffusion field, we hypothesized that the application of an external electric field could affect self-assembly of the membrane.(Figure 1 B,C) Electric fields have been widely used in various other applications, e.g., for electrophoresis,[16] electrophoretic deposition,[17] to align nanofibers,[18] to orient liquid-crystalline molecules,[19a,b] to manipulate nanoparticles and biomolecules,[20] to control physical,[21] magnetic[22] and optical[23] properties and for various therapeutic uses involving the manipulation of living cells.[24a,b] To accomplish our goal, we implemented the superposition of the intrinsic osmotic forces of the system with an externally applied electric field. The specific approach in this work has been not only to control the strength of the field but also the three-dimensional spatial electric field profiles by changing the electrode geometry. The structure of the closed membranes produced under the field has been studied by electron microscopy and we have also probed their mechanical properties using membrane inflation techniques we reported earlier.[25]

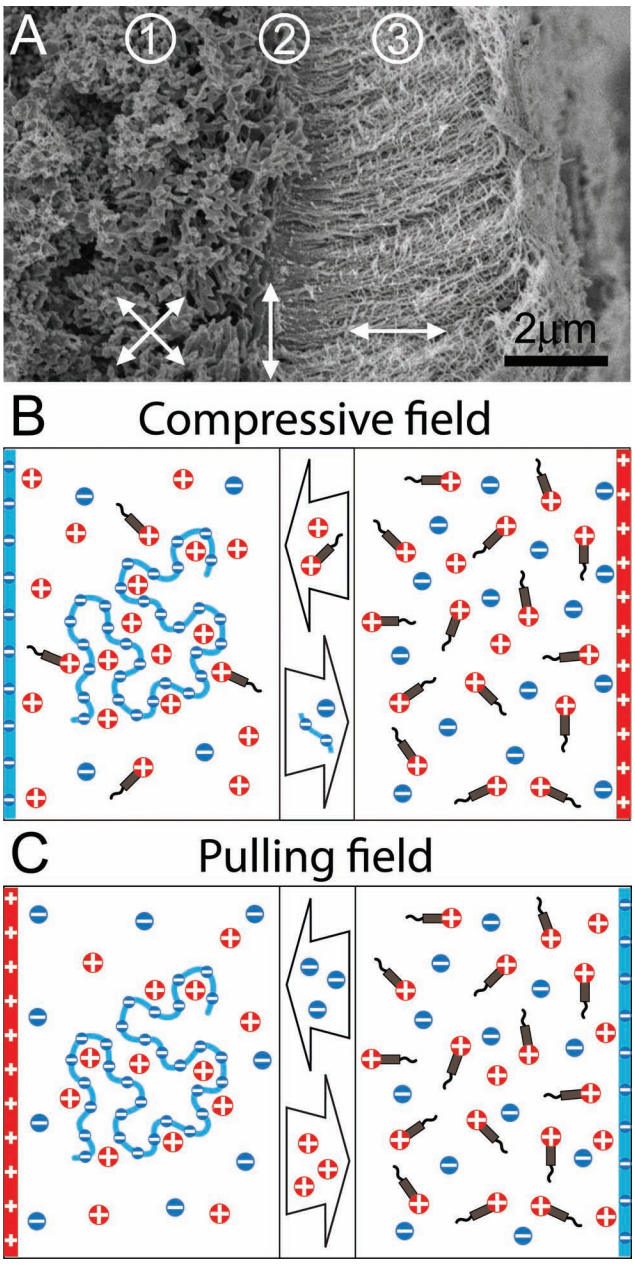

Figure 1. A) SEM image of the PA-HA membrane demonstrates three structurally different layers: (1) an amorphous layer, (2) a narrow region with fibers parallel to the interface and (3) a layer of fibers perpendicular to the interface. Schematic illustration of the electric field setup; B) compressive field to promote diffusion of HA and PA molecules toward the interface and C) pulling field to suppress diffusion.

2. Results and Discussion

2.1. Theory

Dynamics and kinetics of aggregation in the PA-HA systems are considerably influenced by the charged nature of both components and the ability of PA molecules to form high aspect ratio and condensed nanofibers upon screening of charged groups. When the two solutions are brought into contact, their components create a reaction-diffusion field,[26a,b] where dynamic balance between directional diffusion and aggregation of interpenetrating molecular fronts determines the distinctive course of the self-assembly process. The term reaction is used in this manuscript in context of the molecular aggregation or self-assembly. According to nucleation theory,[27a,b] the mechanism of molecular aggregation includes direct and reverse transitions of aggregates through the adsorption and emission of single molecules or small clusters. For example, self-assembly in a two-component (A and B) system could be characterized by a number of aggregation reactions of the type $A_k B_l + A_m B_n \leftrightarrow A_{k+m} B_{l+n}$, where the stoichiometric coefficients k, l, m and n are arbitrary positive integer numbers. The structure and properties of each aggregate depend on the mechanism of the aggregation and intermolecular forces characteristic to the system. PA molecules self-assemble into long cylindrical nanofibers that support continuous growth similar to polymerization.[13a,28] Therefore, we assume that the aggregation products are non-inert and capable of participating in further reactions.

Among all forces, long-range electrostatic interactions significantly affect the molecular mobility that includes the

diffusive flux arising from concentration gradients, $D\vec{\nabla}\rho$ and the charge transference, $ez\mu\rho\vec{E}$, where $\mu = D/k_BT$ is the hydrodynamic mobility, D is the diffusion coefficient, e is the charge of the electron, z is a corresponding charge valence and $\vec{E} = \vec{E}_{loc} + \vec{E}_{ext}$ is the electric field, a sum of local and external components. The local field is created by molecular charges and $\vec{\nabla}\cdot\vec{E}_{loc} = \rho/\varepsilon_o\varepsilon$, where $\rho = \sum z_i\rho_i$ is the local charge density at the current position and $\varepsilon_o\varepsilon$ is the relative permittivity of the media. The external field, on the other hand, is applied to the system, $\vec{\nabla}\cdot\vec{E}_{ext} = 0$ and can be easily controlled. The superposition of local and external electric fields, therefore, suggests an attractive way to interact with the system and gain control over the self-assembly process.

Consequently, the system of the macroscopic equations of motion for each of the diffusing and interacting charged aggregate in the presence of an external electric field can be expressed as follows,

$$\frac{\partial}{\partial t}\rho[\bar{n}] = \acute{D}\Delta\rho[\bar{n}] + J[\bar{n}] + e\acute{\mu}\acute{z}\vec{\nabla}\rho[\bar{n}]\cdot\left(\vec{E}_{loc} + \vec{E}_{ext}\right) - \frac{e\acute{\mu}}{\varepsilon_o\varepsilon}\acute{z}\rho[\bar{n}]\sum_{\bar{m}}\acute{z}[\bar{m}]\rho[\bar{m}] \quad (1)$$

Since aggregates consist of different numbers of PA and HA molecules, here we use two-parameter notation, a vector $\bar{n} = [n_A, n_B$, to represent the composition of the aggregates, i.e. the number of molecules of each type, n_A and n_B, the aggregate consists of. Consequently, $\acute{D} \equiv D[\bar{n}]$ is the diffusion coefficient of the aggregate consisting of n_A molecules of A-type and n_B molecules of B-type, $\acute{z} \equiv z[\bar{n}] = n_Az_A - n_Bz_B$ is the net valence and $\acute{\mu} \equiv \mu[\bar{n}]$ is the hydrodynamic mobility. Summation in the last term is carried over surrounding aggregates $(\bar{m})$. The second term of the equation, $J[\bar{n}]$, describes the flux of aggregates[27b] that directly depends on the mechanism of molecular aggregation and can be written in a general form as:

$$J[\bar{n}] = \sum_{|\delta\bar{n}|Z<|\bar{n}|} k^+[\bar{n}-\delta\bar{n}|\delta\bar{n}]\rho[\bar{n}-\delta\bar{n}]\rho[\delta\bar{n}] + \sum_{|\delta\bar{n}|>0} k^-[\bar{n}+\delta\bar{n}]\rho[\bar{n}+\delta\bar{n}|\delta\bar{n}] - \sum_{|\delta\bar{n}|>0} k^+[\bar{n}|\delta\ ]\rho[\bar{n}]\rho[\delta\bar{n}] - \sum_{|\delta\bar{n}|<|\bar{n}|} k^-[\bar{n}|\delta\bar{n}]\rho[\bar{n}] \quad (2)$$

where $\rho[\bar{n}]$ is a concentration of $\bar{n}$ -aggregates, $k^+[\bar{n}-\delta\bar{n}|\delta\bar{n}]$ determines the rate of association of monomers or small $\delta[\bar{n}]$ -aggregates with the aggregates of size $[\bar{n}-\delta\bar{n}]$ and $k^-[\bar{n}|\delta\bar{n}]$ determines the rate of monomer emission or dissociation of small $[\delta\bar{n}]$ -aggregates by the larger aggregates of size $[\bar{n}]$. Both association $k^+[\cdot]$ and dissociation $k^-[\cdot]$ constants depend on the mechanism of molecular aggregation.[27b]

The system of reaction-diffusion Equation (1) shows the interconnected nature of the kinetics of aggregation and, at the same time, demonstrates how the external electric field can affect the molecular self-assembly and thus, the structure and properties of the forming membrane. While the first two terms, diffusivity and aggregation, are well-known, the last two terms describe contributions from the interactions with the external electric field and the charged environment. Interestingly, the external electric field contribution comes from the dot product of the diffusive flux, $\vec{\nabla}\rho$ and the total electric field, $\vec{E}_{loc} + \vec{E}_{ext}$ and depends on the orientation of both components. This suggests that the external electric field can promote or suppress diffusion of the charged molecules through the interface thus affecting the course of the self-assembly process. This conclusion is also applicable to any charge heterogeneities in the systems, such as aggregates. It is reasonable to assume that the aggregates are nearly electroneutral with exception of the ends that are still "active" and they could have an excess of charge. Therefore the directed migration of molecules and interaction of aggregates with the field could control the direction of nanofiber growth and, thus, affect the structure of the membrane. Furthermore, the interaction of charged aggregates with the electric field could promote separation of aggregates depending on the accumulated charge, thus supporting the formation of dissipative structures. This would reasonably predict a development of various charge heterogeneities within the membrane[29] and possible formation of surface structures[30] or patterns[31] in the presence of the external electric field.

2.2. Experimental Results

We found that the thickness and the structure of the membrane changed significantly when we stimulated the membrane with an external electric field of defined strength and polarity. Our first set of experiments was performed on the closed, spherical membrane sac. **Figure 2**A shows the schematics of the "two-ring" electrode that creates an approximately radial electric field and is convenient to stimulate closed membrane sacs. The sac is located at the center between two connected platinum rings, while another platinum "point" electrode is introduced at the center of the sac and is positioned at the center of the two-ring electrode. Since HA molecules are negatively charged and PA molecules are positively charged, the compressive electric field will promote the diffusion of HA and PA molecules toward the interface, while the pulling field will discourage their diffusion (Figure1 B–C). However, it is also important to mention here the role of small ions, since excess osmotic pressure of ions across the membrane is the primary driving force of the membrane growth. In the presence of large macroions, the counterions can be classified as free or condensed.[32a–c] While the free ions can quickly establish chemical equilibrium, the presence of oppositely charged macroions will restrict the mobility of condensed counterions due to the requirement of electroneutrality. Therefore, application of the external electric field is expected to affect the distribution of small ions and, as a result, the excess osmotic pressure of ions.

Figure 2B–G shows the structure of the sac membranes formed by 0.5 and 1.0 wt% HA and 2.0 wt% PA in which growth was stimulated by electric fields of different strength and polarity for 15 minutes. The PA-HA membrane consists of three layers: an amorphous layer in the biopolymer compartment, a layer of nanofibers parallel to the interface in the middle of the membrane and a layer of fibers perpendicular to

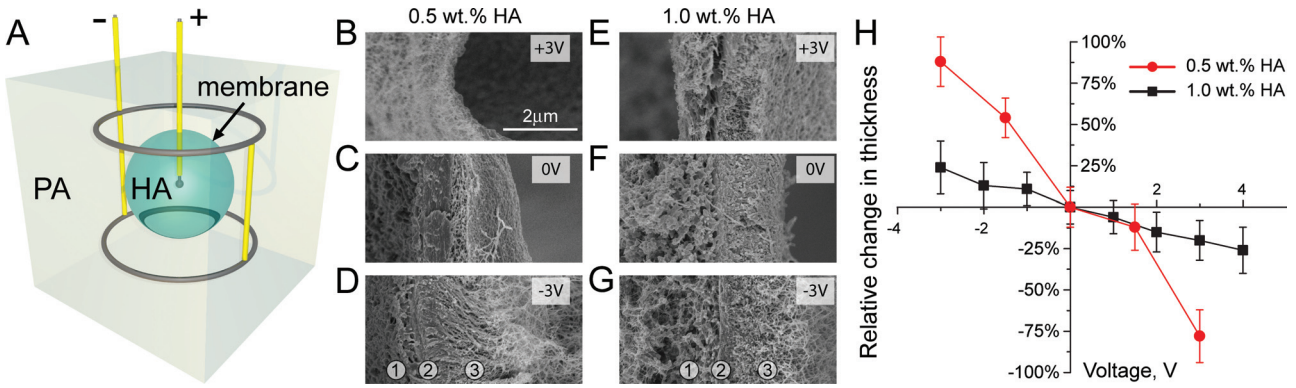

Figure 2. A) Schematic illustration of the "two-ring" electrode corresponding to the "compressive field" voltage setup. The enclosed membrane is shown as a blue sphere, insulated wires as yellow cylinders and naked wires as gray cylinders. B–G) SEM images of the stimulated membrane made from 2wt% PA and (B–D) 0.5 and (E–G) 1 wt% HA. Membranes consist of (1) an amorphous layer, (2) a narrow region with fibers parallel to the interface and (3) a layer of fibers perpendicular to the interface. (H) Relative change in the thickness of the membrane as a function of applied voltage.

the interface that appears approximately 10 minutes after the first contact.[11] Since the region with perpendicular nanofibers develops over time after the rapid formation of the first two regions, we estimated changes in the thickness of the region with parallel and perpendicular nanofibers as a marker of how strongly membrane growth was affected by the electric field. One can see that the membranes stimulated by the compressive field (see Experimental section for details) are more mature (Figure 2D and G) and have structures similar to membranes matured for longer times without stimulation. On the other hand, membranes stimulated by pulling fields have a less developed structure. Figure 2H shows the relative change in the overall membrane thickness calculated as an average from SEM images of sac membrane cross sections. In addition, **Table 1** provides the estimated thicknesses of the membranes as a function of applied voltage for two polymer concentrations. A clear trend is observed of an increasing membrane thickness as the electric field changes polarity from a pulling to a compressive configuration. Due to several potential sources of error in thickness measurements such as differences in the tearing angle of the sac membrane to expose its cross section or the angle between the cross section and the electron beam, the trend of increasing thickness in cross section with stronger compressive fields was not statistically significant in the case of sacs formed with 1.0 wt% HA. Since osmotic pressure forces are the primary driving force for self-assembly in this system, we hypothesized that in the 1.0 wt% HA case where the osmotic pressure difference between the two compartments is large, these forces could be dominating over those produced by the external electric field. We therefore repeated the experiments in 0.5 wt% HA systems, which we have shown previously to produce cross sections that are less mature and less thick due to reduced osmotic pressure forces.[25] Through SEM analysis of stimulated samples in this lower concentration system we found much more pronounced changes in structure and thickness. Depending on the strength and orientation of the field we observe an approximately linear relative change in membrane thickness, particularly up to nearly 100% for 0.5 wt% HA compared to 25% for 1 wt% HA (Figure 2H).

Table 1. Average thickness of the membrane as a function of voltage estimated from analysis of scanning electron microscopy images. Standard deviation is estimated not to exceed 20% of the value and is smaller for thicker membranes.

Voltage, [V]	Thickness, [μm] 1 wt.% HA	Voltage, [V]	Thickness, [μm] 0.5 wt.% HA
4	1.12		
3	1.21		
2	1.30	3	0.20
1	1.43	1.5	0.78
0	1.52	0	0.89
–1	1.69	–1.5	1.38
–2	1.72	–3	1.68
–3	1.88		

We designed additional experiments to see if the structure of membranes could be altered in a manner other than just encouraging or discouraging the diffusion of HA molecules through the initial interface by applying electric fields perpendicular to this interface. Taking into account that the diffusive flux and electric field are coupled through the dot product (see **Equation 1**), we hypothesized that the orientation of the external field could affect the direction of growing nanofibers. To test this prediction, we designed a new experimental setup in which the external electric field was parallel to the HA/PA interface. **Figure 3**A shows the corresponding schematics of the square electrode of 25 × 25mm in size, which creates an approximately constant electric field in the plane of the membrane. SEM microscopy images revealed dramatic changes in the structure of the membrane as the applied voltage was increased. Figure 3B shows the structure of the canonical membrane formed after 30 minutes of incubation without the electric field stimulation. These membranes are very homogeneous in general and display the same structure along the membrane. On the other hand we found that stimulated membranes contained

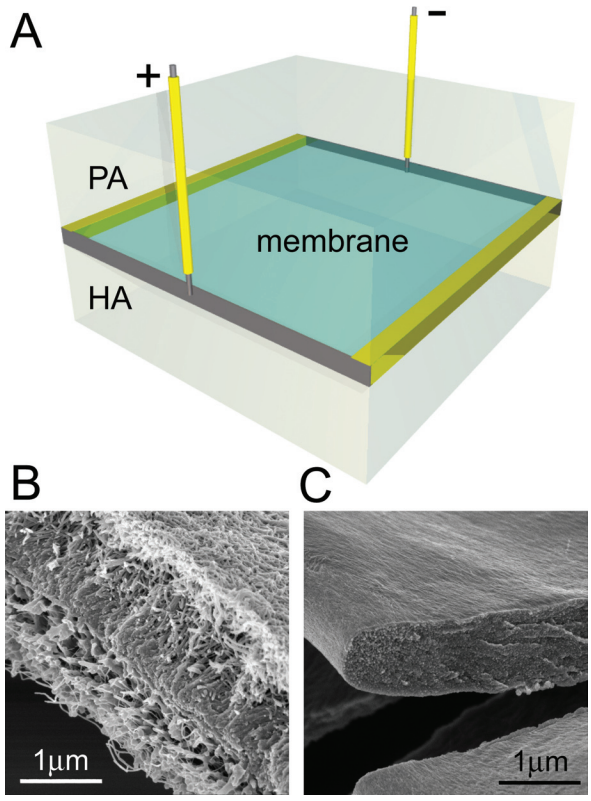

Figure 3. (A) Schematic illustration of the 2D "square" electrode. (B) SEM image of a 30 min membrane formed without stimulation. (C) SEM microscopy image of a 30 min membrane formed with 4V stimulation.

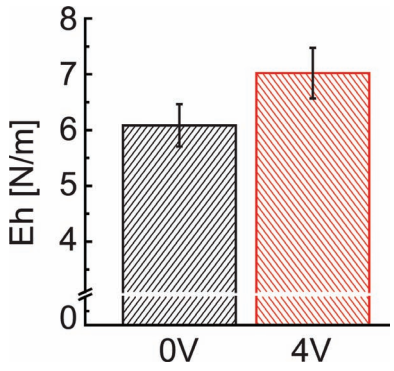

Figure 4. Area modulus of 30 min membranes formed without and with application of an electric field (4V) using the 2D "square" electrode.

structurally different regions including some sections with a structure very similar to that of a canonical membrane. In other regions, however, the structure was very homogenous in thickness and highly dense. Nanofibers parallel to the interface, rather than perpendicular, were found across this region and also seemed to be highly aligned with the direction of the electric field (Figure 3C). The size of these regions was found to be much larger than $100 \times 100\ \mu m^2$. Based on our observations, we hypothesize that the local structure of the membrane changes depending on the strength and orientation of the local electric field.

Using the square electrode, large stimulated membranes, which are amenable for use in membrane inflation experiments, were produced. To assess the effect of the applied electric field on membrane mechanical properties, deformation as a function of pressure was recorded for a set of stimulated and non-stimulated membranes that were incubated for 30 minutes. We have observed that stimulated membranes seem to possess less local defects allowing them to more reliably inflate to high pressures. By fitting the obtained stress-strain curves with a simple neo-Hookean model[33] described previously,[25] we calculated the area modulus of both stimulated and unstimulated membranes. Analysis of the data shows that stimulated membranes have an area modulus which is about 15% greater than that of unstimulated ones (**Figure 4**). Taking into account that the stimulated membranes appear to be thinner in SEM images, the Young's modulus of these membranes should be significantly higher than that of membranes not exposed to the field. In particular, using an estimated thickness of 2 μm and 1.2 μm for the unstimulated membrane and the one stimulated by 4V electric field, we approximate the Young modulus for these samples to be 3.1 and 5.8 MPa, respectively. We believe that this increase in modulus can be attributed to the regions of densely packed fibers aligned in the plane of the membrane. In these regions the local electric field causes parallel orientation of what would normally be perpendicular fibers thereby greatly enhancing their resistance to deformation through what we assume to be alignment-related strengthening mechanisms.[34]

The presence of structurally different regions within the same membrane suggests the existence of transient regions, where one structure changes into another or, in other words, the presence of structural gradients. To investigate this assumption further, we designed another similar system where one electrode is a 10 mm ring in the plane of the membrane and another point electrode is at the center of the ring electrode (**Figure 5**A). This setup significantly changes the electric field profile, making it radial in the plane of the membrane and decaying in strength with the distance from the center, promoting the development of varying structures along the field. Again, SEM analysis revealed different structures throughout the membrane. While a relatively weak field near the outer electrode leaves the membrane structure unchanged (Figure 5B), i.e. fibers grow along a direction perpendicular to the membrane or the field, we also found regions with fibers aligned with the field orientation (Figure 5C) without any evidence of the perpendicularly growing fibers observed in a normal membrane. These structures look similar to the structures found in the previous case (Figure 3C). Thus, by using an electrode that creates a 2D radial field it is possible to create a self-assembled membrane with a structural gradient pattern, where the orientation of the fibers was changing from parallel to the membrane surface to perpendicular as a function of distance from the center electrode.

While canonical PA-HA membranes are known to be flat and smooth on macroscopic scales, among those stimulated with a strong electric field we found some regions with

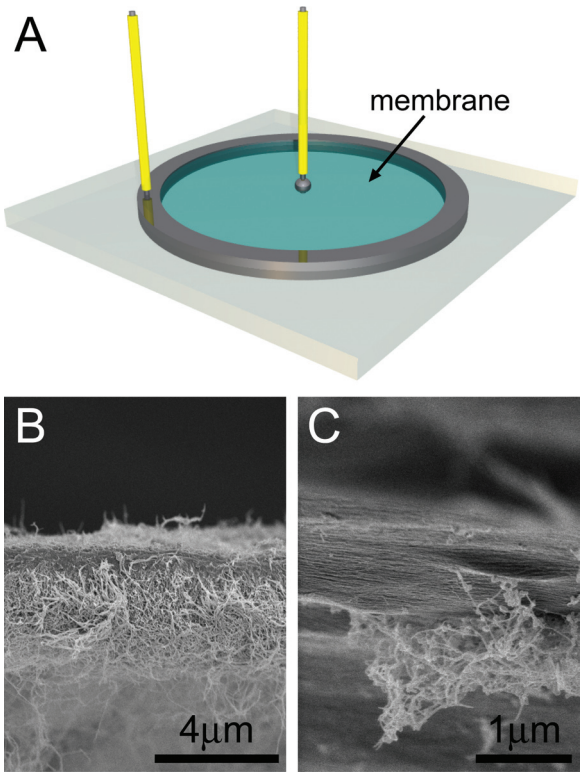

Figure 5. A) Schematic illustration of the 2D "ring" electrode setup. SEM image of B) region near the outside of the membrane where the field is weak and C) region near the center of the membrane where the field is strongest with parallel nanofibers.

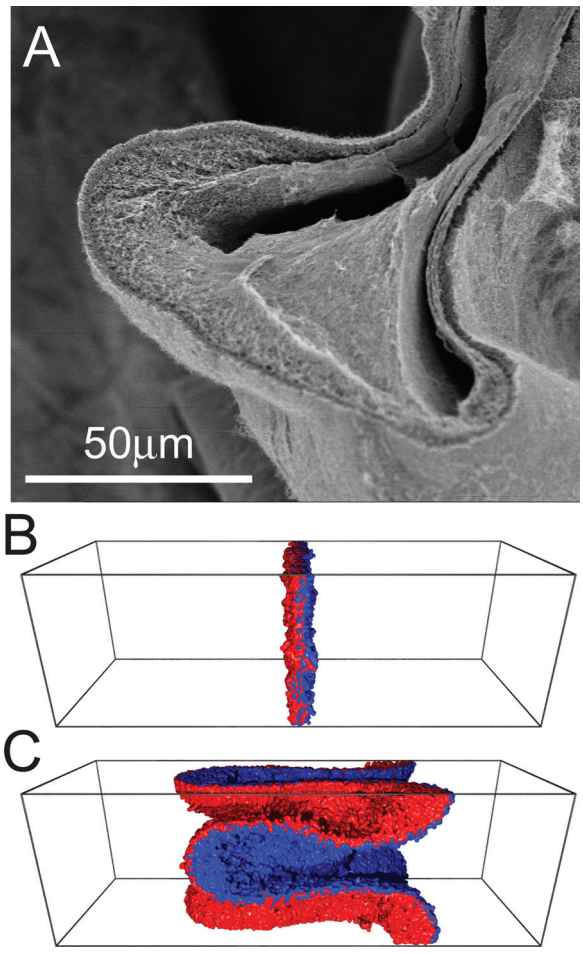

Figure 6. A) SEM image of the surface structure formed under compressive electric field (-3V, 15min) created by "two-ring" electrode. Molecular dynamics simulation snapshot of the membrane formed (B) without ($E_o = 0$) and (C) with compressive field stimulation ($E_o = 0.1$).

undulated structure and surface patterns (**Figure 6**A). These undulated structures display the same features observed in canonical membranes. However, the membrane as a whole adopts an undulated shape which must be connected to local heterogeneities in charge distributions. It was demonstrated recently that an external electric field can induce instability at air-polymer film interfaces,[30] driving the formation of similar undulated structures. This phenomenon was attributed to the competition between a destabilizing electrostatic energy and a stabilizing elastic energy of the polymer film. We believe that a similar phenomenon occurs in self-assembled membranes. However, the complex supramolecular structure of the membrane appears to lock in place the undulated structure even when the field is removed. In the case of the amorphous polymer films the undulation disappears as soon as the field is removed. We have also performed molecular simulations based on the theoretical model discussed above to study membrane formation under the influence of external fields.[35] All details on the computational model can be found in the Experimental section and ref. [35] Briefly, we considered a system of two solutions initially separated by the interface and each composed of molecular components of only one kind, A or B. When solutions are brought into the contact, the molecules diffuse toward each other and start to interact, according to the formula $nA + mB \rightleftarrows A_n B_m$, where the stoichiometric coefficients n and m are positive integer numbers. In the field-free case a solid planar membrane is formed at the interface (Figure 6B). However, application of the compressive field results in the formation of large undulations (Figure 6C) in the membrane, which confirms our experimental findings. While this finding is clearly beyond the scope of this work, it suggests a new way for creating membranes with complex surface structures and patterns.

3. Conclusions

We have investigated the superposition of an electric field in a process of dynamic self-assembly forming a membrane at the interface of an aqueous solution of positively charged supramolecular nanostructures and an aqueous solution of an anionic polyelectrolyte. The superposition of an external electric field in a field of molecular co-assembly and diffusion of the charged species allows control of both growth rate and directionality of the fibrils that make up the membrane. The strategy can be of general use in the control of structure and physical properties of charged self-assembling systems in water.

4. Experimental Section

Materials: The molecular weight of HA used in all experiments had an average molar mass of 1.76 mDa and was purchased from Lifecore Biomedical, Inc (Chaska, MN).

PA Synthesis/Purification: C16–V3A3K3–NH2 peptide amphiphiles were synthesized as previously described[36] by standard Fmoc solid phase peptide synthesis and purified using reverse phase high performance liquid chromatography with a mobile phase gradient consisting of water and acetonitrile, each containing 0.1% v/v trifluoroacetic acid (TFA).

Electric Field Stimulation: Spherical sac membranes exposed to electric fields were created in 5mm square cuvets and visualized during experiments with a Kruss DSA100 drop-shape analysis apparatus. External electric fields were generated by applying voltage to two separate electrodes: one external "double-ring" electrode with loops above and below the sac and another electrode inside the sac in the biopolymer compartment. The diameter of the ring electrode and the distance between two rings were equal to 4mm. This configuration of electrodes produces an electric field radiating outward from the interior electrode at the center of the sac, perpendicular to the plane of the interface of the two solutions (Figure 2). In order to achieve this configuration, the "double-ring" electrode was placed into the cuvet and PA solution was pipetted in, to a level near the midpoint of the two rings. An 8 µL droplet of HA was then brought into contact with the surface using the dispensing and motor controls of the DSA. Surface tension drags this viscous droplet down into the PA solution but it is quickly stabilized in place by the initial self-assembly and formation of the membrane. This sac is not fully enclosed with the biopolymer compartment open to the air at the surface,[25] allowing for the insertion of the second electrode into the sac. This electrode is placed inside the needle of a PA-filled syringe and is insulated up until the very tip. PA is dispensed from the syringe and self-assembles with the biopolymer open to the air, completing the enclosure of the sac and trapping the second electrode inside. More PA solution is dispensed to ensure that the entire sac and the 'double-ring' external electrode are submerged. A voltage is applied with a USB-1408FS analog in/out module (Measurement Computing) controlled by a custom-written visual basic program.

To stimulate the large flat membrane sizes required for membrane inflation characterization, we created new planar electrodes from 127 µm thick 99.99% pure platinum foil (Alfa Aesar). A plastic washer (OD: 25 mm, ID: 23 mm, height: 2 mm) was placed on top of one flat electrode and filled with 850 µL of biopolymer solution. 300 µL of PA solution was dropped on top and gently distributed across the surface of the biopolymer to ensure membrane formation across the entire diameter of the washer as well as adhesion to the inner ring of the washer for washing steps. The top flat electrode was placed on top of the washer, in contact with the excess PA solution and the voltage was applied. After the period of stimulation, electrodes were carefully removed and membranes were inflated as described in the 'membrane inflation' section and previously.[25]

The geometry of the electrodes and the applied voltage both determine the strength and the structure of the electric field. To achieve desired field geometries, we utilized the combination of naked and insulated wires in various configurations. We used electrodes of different shape that create 3D radial (Figure 2A), planar (Figure 3A) and 2D radial (Figure 5A) electric fields. We estimate the strength of the electric field used in our experiments varies in the range from 0 to 250 Vm^{-1}, corresponding to applied voltages from 0V to +4V. For simplicity, we identify the field created by the negatively charged electrode in the HA compartment and positively charged electrode in the PA compartment as a "compressive" field and the reverse configuration as a "pulling" field (Figure 1B,C).

Scanning Electron Microscopy: After the desired maturation time, materials were fixed in 4% glutaraldehyde with 3% sucrose and dehydrated in serial dilutions of ethanol in water, from 20% to 100%. Critical point drying was performed with a Tousimis SAMDRI-795 critical point dryer. Dry samples were then manually torn to expose the cross section for imaging and placed on conductive adhesive tabs on pin stubs (Ted Pella). Metal coating for imaging was done with an osmium plasma coater (Structure Probe, Inc.) with a nominal coating thickness of 15nm. Samples were then imaged in a Hitachi S-4800 field emission scanning electron microscope with a typical acceleration voltage of 2.0kV to emphasize surface features.

Membrane Inflation: Membranes (5 per group) for membrane inflation were formed in circular polystyrene washers (inner diameter = 20 mm) or in a square electrode (20 mm × 20 mm) by filling with 950 mL of the HA solution and adding 300mL of PA on top of the biopolymer solution. The PA solution was spread with a glass slide to form a continuous layer to ensure a complete membrane across the washer. Membranes were incubated at room temperature for either 15, 30 or 60 minutes then rinsed carefully with nanopure water to remove excess biopolymer and PA. Inflation of the membrane was completed as described previously.[25] The membrane was carefully transferred from the washer to a metal holder and secured with a ring clamp. A few drops of water were added on top of the membrane to ensure hydration. The sample in the holder was placed on a custom-built apparatus for membrane inflation. Inflation was controlled with a syringe pump (New Era Pump Systems) and images were recorded with a B&W camera (Adimec) to monitor deformation while pressure was measured using a pressure sensor (MKS instruments). The area modulus, given by Eh where h is the membrane thickness and E is the average Young's modulus through the thickness, was determined using a neo-Hookean model.[33]

Computational Model: To study aggregation at the interface between two miscible solutions, the following computational model was used. We consider a system of two solutions each composed of molecular components of only one kind, A or B, dissolved in the same solvent and initially separated by the interface. Each molecule is described as a polymer chain of length, N that was varied from 1 to 32. We also assume that all monomers have equal size, σ mass, m and diffusivity. The simulation was performed in a rectangular box with dimensions of $L_X \times L_Y \times L_Z$, where the original interface is parallel to the XZ-plane and is located in the center of the box along Y-direction. Periodic boundary conditions[37a,b] are applied in the X and Z directions. However, the choice of boundary conditions (BCs) for the Y-direction is less obvious. To incorporate the proper BCs described above, we employed dual control volume grand canonical molecular dynamics with the streaming velocity method.[38a–e] Thus, in our case, the simulation system consists of three interacting compartments (**Figure 7**A): one at the center (C-compartment) and two on both sides along the Y-direction (BC-compartments). Each BC-compartment is in direct contact with the C-compartment on a side that does not restrict molecular movement. On the other hand, the opposite boundary is considered as a hard wall. Thus, each BC-compartment can exchange molecules with C-compartment so that constant densities of molecules at the corresponding boundaries of the C-compartment along the Y-direction can be fulfilled. This model, however, is limited by the width of the C-compartment. In particular, it assumes that the reaction zone is localized far from each BC-compartment and that the thickness of the reaction zone does not exceed the length of the C-compartment. The dimensions of the whole simulation box were chosen as $L_X = L_Z = 80\sigma$ and $L_Y = L_Y^A + L_Y^B$ (from $-L_Y^A$ to L_Y^B), where $L_Y^A = L_Y^B = 100\sigma$. To avoid significant density fluctuations in BC-compartments the length along the Y-direction was chosen to be equal: $\delta L_Y = \delta L_Y^A = \delta L_Y^B = 20\sigma$. We assume that in the beginning both solutions are in equilibrium at the same temperature and pressure and molecules are distributed uniformly in the volume and in close proximity to the interface. Thus, at the time moment $t = 0$, corresponding initial conditions (ICs)

$$\rho_A(y, 0) = \rho_A^o H(-y),$$
$$\rho_B(y, 0) = \rho_B^o H(y), \quad (3)$$

and boundary conditions (BCs)

$$\rho_A(-L_Y^A + \delta L_Y, t) = \rho_A^o,$$
$$\rho_A(L_Y^B - \delta L_Y, t) = 0,$$
$$\rho_B(L_Y^B - \delta L_Y, t) = \rho_B^o,$$
$$\rho_B(-L_Y^A + \delta L_Y, t) = 0, \quad (4)$$

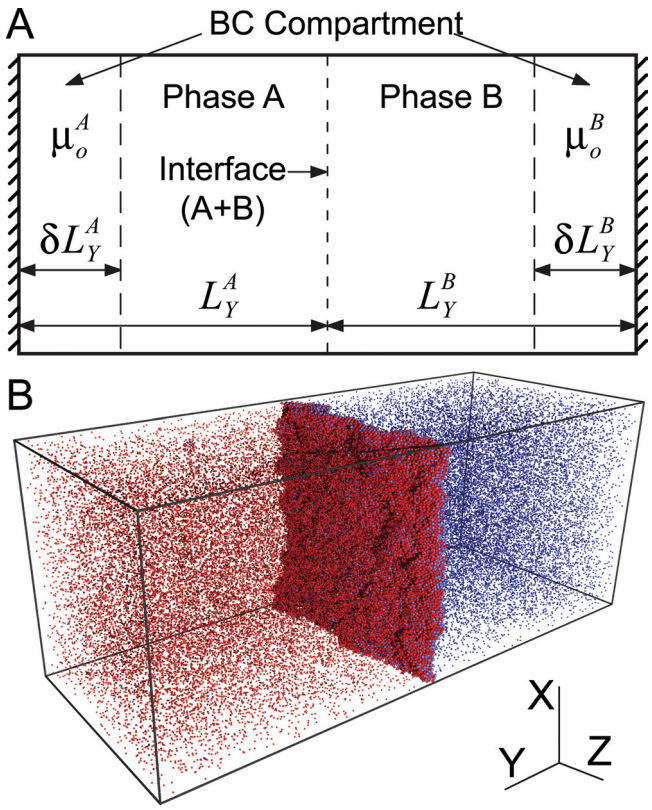

Figure 7. A) Schematic of a computational model consisting of two BC-compartments to utilize appropriate boundary conditions and a central C-compartment where two solutions create a nascent interface. Each BC-compartment is in direct contact with the C-compartment on a side that does not restrict molecular movement. Periodic boundary conditions are applied in the X and Z directions, while both outer boundaries in the Y direction are modeled as a hard wall. (B) Snapshot of the membrane formed near the original interface after $t \approx 1000$ time steps in the system at $\rho_0 = 0.1\sigma^{-3}$ and $\varepsilon_{AB} = 8k_BT$.

where $H(\gamma)$ is the Heaviside unit step function, $\rho_A(\gamma, t)$ and $\rho_B(\gamma, t)$ are the densities of A and B molecular components at the position y and time moment t correspondingly. For the sake of simplicity, we study a symmetric system assuming that the initial local densities in each compartment are equal, $\rho_A^o = \rho_B^o = \rho_o$. We studied a number of systems with the number density varying in the range from $0.01\sigma^{-3}$ to $0.3\sigma^{-3}$.

A simulation was carried out within the framework of mixed Monte Carlo and stochastic dynamics. The stochastic dynamics simulation is performed in Cartesian space by solving Langevin's equations using the Langevin dynamics velocity Verlet method:[37a,b]

$$m_i \frac{d^2\vec{r}_i}{dt^2} = -\frac{\partial U(\vec{r}_i, t)}{\partial r} - \gamma m_i \frac{d\vec{r}_i}{dt} + \vec{\Gamma}_i(t) \quad (5)$$

where m_i is the mass and $\vec{r}_i$ is the position vector of the i th particle, $U(\vec{r}_i, t)$ is the total potential affecting the particle, $\gamma = 1$ is the friction coefficient (damping constant in reciprocal time units) and $\vec{\Gamma}_i(t)$ is a stochastic force satisfying the conditions of Gaussian white noise $\langle \vec{\Gamma}_i(t)\vec{\Gamma}_i(\acute{t})\rangle = 2\gamma m_i k_B T \delta(t - \acute{t})$, where k_B is Boltzmann's constant, T is the temperature and $\delta(\cdot)$ the delta-function. The interactions between A and B particles were modeled with a short range Morse potential:

$$U_{AB}(r_{ij}) = \varepsilon_{AB}\left(\exp\left[-2\alpha\frac{r_{ij} - \sigma}{\sigma}\right] - \exp\left[-\alpha\frac{r_{ij} - \sigma}{\sigma}\right]\right) \quad (6)$$

where ε_{AB} determines the strength of interactions in k_BT units and $r_{ij} = |\vec{r}_i - \vec{r}_j|$. The interactions between identical particles were modeled with a first term that describes excluded volume interactions; e.g. for A-A pair:

$$U_{AA}(r_{ij}) = \varepsilon_{AA}\exp\left[-2\alpha\frac{r_{ij} - \sigma}{\sigma}\right] \quad (7)$$

The constant $\alpha = 24$ determines the shape of the potential and how fast it goes to zero. The interaction energy ε_{AB} was varied in the range from $4k_BT$ to $8k_BT$. The migration of particles in an applied external field, $\vec{E} = \hat{y}E_o$, was modeled by applying an additional potential, $U_f = qE_o$, where q determines an effective particle "charge" set to +1 or −1 for different components, at the same time, assuming non-electrostatic origin of interactions for the sake of computational simplicity.

A Monte Carlo step was performed after each stochastic dynamics step and included the creation or removal of randomly selected particles in BC-compartments.[38c,e] The probability of creation a new particle is given by:

$$\Pi_i^+ = \min\left\{1, Z_i V_{BC} \exp\left(\frac{\Delta E}{k_B T (N_i + 1)}\right)\right\} \quad (8)$$

and

$$\Pi_i^- = \min\left\{1, N_i \exp\left(\frac{\Delta E}{Z_i V_{BC} k_B T}\right)\right\} \quad (9)$$

where $Z_i = \wedge^{-3}\exp(\mu_o^i / k_BT)$ is the absolute activity,[39] $\wedge$ is the de Broglie wavelength, μ_o^i the chemical potential of component i, $V_{BC} = L_X \delta L_Y L_Z$ is the volume and N_i is the number of particles of component i in each BC- compartment and ΔE the energy change due to creating or removing a particle.

Acknowledgements

This work was supported by the Office of Basic Energy Sciences, Materials Sciences and Engineering Division, of the U.S. Department of Energy under Contract No. DE-FG02-00ER45810. J.R.M. was supported by a fellowship from the NIH sponsored Biotechnology Training Program (5T32GM008449) and R.B. received partial support through a postdoctoral fellowship from Ben Gurion University in Israel. Andrew Cheetham from the Chemistry Core of the Institute for BioNanotechnology in Medicine (IBNAM) at Northwestern provided assistance with synthesis and purification of molecules. Experiments in this work made use of EPIC facilities of the NUANCE Center and IBNAM at Northwestern University. The NUANCE Center is supported by the NSF-NSEC, NSF-MRSEC, Keck Foundation and the State of Illinois.

Received: July 7, 2011
Revised: August 28, 2011
Published online: October 6, 2011

[1] a) J. M. Lehn, *Angew. Chem.-Int. Edit. Engl.* **1990**, *29*, 1304; b) S. I. Stupp, V. LeBonheur, K. Walker, L. S. Li, K. E. Huggins, M. Keser, A. Amstutz, *Science* **1997**, *276*, 384; c) L. Brunsveld, B. J. B. Folmer, E. W. Meijer, R. P. Sijbesma, *Chem. Rev.* **2001**, *101*, 4071; d) G. M. Whitesides, B. Grzybowski, *Science* **2002**, *295*, 2418; e) L. C. Palmer, Y. S. Velichko, M. O. de la Cruz, S. I. Stupp, *Philos. Trans. R. Soc. A-Math. Phys. Eng. Sci.* **2007**, *365*, 1417.
[2] T. M. Hermans, M. A. C. Broeren, N. Gomopoulos, P. van der Schoot, M. H. P. van Genderen, N. Sommerdijk, G. Fytas, E. W. Meijer, *Nat. Nanotechnol.* **2009**, *4*, 721.

[3] H. G. Cui, Z. Y. Chen, S. Zhong, K. L. Wooley, D. J. Pochan, *Science* **2007**, *317*, 647.
[4] S. M. Zhang, M. A. Greenfield, A. Mata, L. C. Palmer, R. Bitton, J. R. Mantei, C. Aparicio, M. O. de la Cruz, S. I. Stupp, *Nat. Mater.* *9*, 594.
[5] C. Wang, Y. S. Guo, Y. P. Wang, H. P. Xu, R. J. Wang, X. Zhang, *Angew. Chem.-Int. Edt.* **2009**, *48*, 8962.
[6] F. J. Nedelec, T. Surrey, A. C. Maggs, S. Leibler, *Nature* **1997**, *389*, 305.
[7] D. A. Fletcher, D. Mullins, *Nature 463*, 485.
[8] M. Takinoue, Y. Atsumi, K. Yoshikawa, *Appl. Phys. Lett.* **2010**, *96*.
[9] H. G. Cui, E. T. Pashuck, Y. S. Velichko, S. J. Weigand, A. G. Cheetham, C. J. Newcomb, S. I. Stupp, *Science* **2010**, *327*, 555.
[10] B. A. Grzybowski, H. A. Stone, G. M. Whitesides, *Nature* **2000**, *405*, 1033.
[11] R. M. Capito, H. S. Azevedo, Y. S. Velichko, A. Mata, S. I. Stupp, *Science* **2008**, *319*, 1812.
[12] a) J. D. Hartgerink, E. Beniash, S. I. Stupp, *Proc. Natl. Acad. Sci. U.S.A.* **2002**, *99*, 5133; b) H. A. Behanna, J. Donners, A. C. Gordon, S. I. Stupp, *J. Am. Chem. Soc.* **2005**, *127*, 1193; c) H. G. Cui, M. J. Webber, S. I. Stupp, *Biopolymers* **2010**, *94*, 1.
[13] a) Y. S. Velichko, S. I. Stupp, M. O. de la Cruz, *J. Phys. Chem. B* **2008**, *112*, 2326; b) O. S. Lee, S. I. Stupp, G. C. Schatz, *J. Am. Chem. Soc.* **2011**, *133*, 3677.
[14] G. S. Manning, *Annu. Rev. Phys. Chem.* **1972**, *23*, 117.
[15] M. Deserno, H. H. von Grunberg, *Phys. Rev. E* **2002**, *66*, 15.
[16] M. Bier, *Electrophoresis: Theory, Methods, and Applications*, Academic Press, New York **1959**.
[17] P. Sarkar, P. S. Nicholson, *J. Am. Ceram. Soc.* **1996**, *79*, 1987.
[18] Y. Cao, W. Liu, J. L. Sun, Y. P. Han, J. H. Zhang, S. Liu, H. S. Sun, J. H. Guo, *Nanotechnology* **2006**, *17*, 2378.
[19] a) D. Miyajima, F. Araoka, H. Takezoe, J. Kim, K. Kato, M. Takata, T. Aida, *Angew. Chem. Int. Edt.* **2011**, *50*, 7865; b) K. Sato, Y. Itoh, T. Aida, *J. Am. Chem. Soc.* **2011**, null.
[20] Y. L. Liu, K. Oh, J. G. Bai, C. L. Chang, W. Yeo, J. H. Chung, K. H. Lee, W. K. Liu, *Comput. Meth. Appl. Mech. Eng.* **2008**, *197*, 2156.
[21] T. Tanaka, I. Nishio, S. T. Sun, S. Uenonishio, *Science* **1982**, *218*, 467.
[22] H. Ohno, D. Chiba, F. Matsukura, T. Omiya, E. Abe, T. Dietl, Y. Ohno, K. Ohtani, *Nature* **2000**, *408*, 944.
[23] F. Meyers, S. R. Marder, B. M. Pierce, J. L. Bredas, *J. Am. Chem. Soc.* **1994**, *116*, 10703.
[24] a) K. R. Robinson, *J. Cell Biol.* **1985**, *101*, 2023; b) J. Voldman, *Annu. Rev. Biomed. Eng.* **2006**, *8*, 425.
[25] D. Carvajal, R. Bitton, J. R. Mantei, Y. S. Velichko, S. I. Stupp, K. R. Shull, *Soft Matter* **2010**, *6*, 1816.
[26] a) G. Nicolis, I. Prigogine, *Self-organization in Nonequilibrium Systems: From Dissipative Structures To Order Through Fluctuations*, Wiley, **1977**; b) J. S. Langer, *Rev. Mod. Phys.* **1980**, *52*, 1.
[27] a) D. Kashchiev, *Nucleation: basic theory with applications*, Butterworth Heinemann, Oxford **2000**; b) J. Schmelzer, *Nucleation Theory and Applications*, Wiley-VCH, Weinheim; Chichester **2005**.
[28] I. A. Nyrkova, A. N. Semenov, *Eur. Phys. J. E* **2005**, *17*, 327.
[29] S. M. Loverde, Y. S. Velichko, M. O. de la Cruz, *J. Chem. Phys.* **2006**, *124*, 7.
[30] E. Schaffer, T. Thurn-Albrecht, T. P. Russell, U. Steiner, *Nature* **2000**, *403*, 874.
[31] N. E. Voicu, S. Harkema, U. Steiner, *Adv. Funct. Mater.* **2006**, *16*, 926.
[32] a) G. S. Manning, *J. Chem. Phys.* **1969**, *51*, 924; b) G. S. Manning, *J. Chem. Phys.* **1969**, *51*, 934; c) G. S. Manning, *J. Chem. Phys.* **1969**, *51*, 3249.
[33] A. L. Flory, D. A. Brass, K. R. Shull, *J. Polym. Sci. Pt. B-Polym. Phys.* **2007**, *45*, 3361.
[34] H. Kang, Q. Wen, P. A. Janmey, J. X. Tang, E. Conti, F. C. MacKintosh, *J. Phys. Chem. B* **2009**, *113*, 3799.
[35] Y. S. Velichko, F. J. Solis, S. I. Stupp, Unpublished.
[36] M. J. Webber, J. Tongers, M. A. Renault, J. G. Roncalli, D. W. Losordo, S. I. Stupp, *Acta Biomater.* **2010**, *6*, 3.
[37] a) D. Frenkel, B. Smit, *Understanding molecular simulation: from algorithms to applications*, Academic Press, **1996**; b) A. R. Leach, *Molecular Modelling: Principles and Applications*, Prentice Hall, **2001**.
[38] a) G. S. Heffelfinger, F. Vanswol, *J. Chem. Phys.* **1994**, *100*, 7548; b) C. M. Lo, B. Palmer, *J. Chem. Phys.* **1995**, *102*, 925; c) L. F. Xu, T. T. Tsotsis, M. Sahimi, *J. Chem. Phys.* **1999**, *111*, 3252; d) G. Arya, H. C. Chang, E. J. Maginn, *J. Chem. Phys.* **2001**, *115*, 8112; e) M. Lisal, J. K. Brennan, W. R. Smith, F. R. Siperstein, *J. Chem. Phys.* **2004**, *121*, 4901.
[39] D. K. Schwartz, J. Garnaes, R. Viswanathan, J. A. N. Zasadzinski, *Science* **1992**, *257*, 508.